

**Measurement of Exclusive $B \rightarrow X_u \ell \nu$ Decays
 with $D^{(*)} \ell \nu$ Decay Tagging**

K. Abe,¹⁰ K. Abe,⁴⁶ N. Abe,⁴⁹ I. Adachi,¹⁰ H. Aihara,⁴⁸ M. Akatsu,²⁴ Y. Asano,⁵³
 T. Aso,⁵² V. Aulchenko,² T. Aushev,¹⁴ T. Aziz,⁴⁴ S. Bahinipati,⁶ A. M. Bakich,⁴³
 Y. Ban,³⁶ M. Barbero,⁹ A. Bay,²⁰ I. Bedny,² U. Bitenc,¹⁵ I. Bizjak,¹⁵ S. Blyth,²⁹
 A. Bondar,² A. Bozek,³⁰ M. Bračko,^{22,15} J. Brodzicka,³⁰ T. E. Browder,⁹ M.-C. Chang,²⁹
 P. Chang,²⁹ Y. Chao,²⁹ A. Chen,²⁶ K.-F. Chen,²⁹ W. T. Chen,²⁶ B. G. Cheon,⁴
 R. Chistov,¹⁴ S.-K. Choi,⁸ Y. Choi,⁴² Y. K. Choi,⁴² A. Chuvikov,³⁷ S. Cole,⁴³
 M. Danilov,¹⁴ M. Dash,⁵⁵ L. Y. Dong,¹² R. Dowd,²³ J. Dragic,²³ A. Drutskoy,⁶
 S. Eidelman,² Y. Enari,²⁴ D. Epifanov,² C. W. Everton,²³ F. Fang,⁹ S. Fratina,¹⁵
 H. Fujii,¹⁰ N. Gabyshev,² A. Garmash,³⁷ T. Gershon,¹⁰ A. Go,²⁶ G. Gokhroo,⁴⁴
 B. Golob,^{21,15} M. Grosse Perdekamp,³⁸ H. Guler,⁹ J. Haba,¹⁰ F. Handa,⁴⁷ K. Hara,¹⁰
 T. Hara,³⁴ N. C. Hastings,¹⁰ K. Hasuko,³⁸ K. Hayasaka,²⁴ H. Hayashii,²⁵ M. Hazumi,¹⁰
 E. M. Heenan,²³ I. Higuchi,⁴⁷ T. Higuchi,¹⁰ L. Hinz,²⁰ T. Hojo,³⁴ T. Hokuue,²⁴
 Y. Hoshi,⁴⁶ K. Hoshina,⁵¹ S. Hou,²⁶ W.-S. Hou,²⁹ Y. B. Hsiung,²⁹ H.-C. Huang,²⁹
 T. Igaki,²⁴ Y. Igarashi,¹⁰ T. Iijima,²⁴ A. Imoto,²⁵ K. Inami,²⁴ A. Ishikawa,¹⁰ H. Ishino,⁴⁹
 K. Itoh,⁴⁸ R. Itoh,¹⁰ M. Iwamoto,³ M. Iwasaki,⁴⁸ Y. Iwasaki,¹⁰ R. Kagan,¹⁴ H. Kakuno,⁴⁸
 J. H. Kang,⁵⁶ J. S. Kang,¹⁷ P. Kapusta,³⁰ S. U. Kataoka,²⁵ N. Katayama,¹⁰ H. Kawai,³
 H. Kawai,⁴⁸ Y. Kawakami,²⁴ N. Kawamura,¹ T. Kawasaki,³² N. Kent,⁹ H. R. Khan,⁴⁹
 A. Kibayashi,⁴⁹ H. Kichimi,¹⁰ H. J. Kim,¹⁹ H. O. Kim,⁴² Hyunwoo Kim,¹⁷ J. H. Kim,⁴²
 S. K. Kim,⁴¹ T. H. Kim,⁵⁶ K. Kinoshita,⁶ P. Koppenburg,¹⁰ S. Korpar,^{22,15} P. Križan,^{21,15}
 P. Krokovny,² R. Kulasiri,⁶ C. C. Kuo,²⁶ H. Kurashiro,⁴⁹ E. Kurihara,³ A. Kusaka,⁴⁸
 A. Kuzmin,² Y.-J. Kwon,⁵⁶ J. S. Lange,⁷ G. Leder,¹³ S. E. Lee,⁴¹ S. H. Lee,⁴¹
 Y.-J. Lee,²⁹ T. Lesiak,³⁰ J. Li,⁴⁰ A. Limosani,²³ S.-W. Lin,²⁹ D. Liventsev,¹⁴
 J. MacNaughton,¹³ G. Majumder,⁴⁴ F. Mandl,¹³ D. Marlow,³⁷ T. Matsuishi,²⁴
 H. Matsumoto,³² S. Matsumoto,⁵ T. Matsumoto,⁵⁰ A. Matyja,³⁰ Y. Mikami,⁴⁷
 W. Mitaroff,¹³ K. Miyabayashi,²⁵ Y. Miyabayashi,²⁴ H. Miyake,³⁴ H. Miyata,³² R. Mizuk,¹⁴
 D. Mohapatra,⁵⁵ G. R. Moloney,²³ G. F. Moorhead,²³ T. Mori,⁴⁹ A. Murakami,³⁹
 T. Nagamine,⁴⁷ Y. Nagasaka,¹¹ T. Nakadaira,⁴⁸ I. Nakamura,¹⁰ E. Nakano,³³ M. Nakao,¹⁰
 H. Nakazawa,¹⁰ Z. Natkaniec,³⁰ K. Neichi,⁴⁶ S. Nishida,¹⁰ O. Nitoh,⁵¹ S. Noguchi,²⁵
 T. Nozaki,¹⁰ A. Ogawa,³⁸ S. Ogawa,⁴⁵ T. Ohshima,²⁴ T. Okabe,²⁴ S. Okuno,¹⁶
 S. L. Olsen,⁹ Y. Onuki,³² W. Ostrowicz,³⁰ H. Ozaki,¹⁰ P. Pakhlov,¹⁴ H. Palka,³⁰
 C. W. Park,⁴² H. Park,¹⁹ K. S. Park,⁴² N. Parslow,⁴³ L. S. Peak,⁴³ M. Pernicka,¹³
 J.-P. Perroud,²⁰ M. Peters,⁹ L. E. Piilonen,⁵⁵ A. Poluektov,² F. J. Ronga,¹⁰ N. Root,²
 M. Rozanska,³⁰ H. Sagawa,¹⁰ M. Saigo,⁴⁷ S. Saitoh,¹⁰ Y. Sakai,¹⁰ H. Sakamoto,¹⁸
 T. R. Sarangi,¹⁰ M. Satapathy,⁵⁴ N. Sato,²⁴ O. Schneider,²⁰ J. Schümann,²⁹ C. Schwanda,¹³
 A. J. Schwartz,⁶ T. Seki,⁵⁰ S. Semenov,¹⁴ K. Senyo,²⁴ Y. Settai,⁵ R. Seuster,⁹
 M. E. Sevier,²³ T. Shibata,³² H. Shibuya,⁴⁵ B. Shwartz,² V. Sidorov,² V. Siegle,³⁸
 J. B. Singh,³⁵ A. Somov,⁶ N. Soni,³⁵ R. Stamen,¹⁰ S. Stanič,^{53,*} M. Starič,¹⁵ A. Sugi,²⁴
 A. Sugiyama,³⁹ K. Sumisawa,³⁴ T. Sumiyoshi,⁵⁰ S. Suzuki,³⁹ S. Y. Suzuki,¹⁰ O. Tajima,¹⁰
 F. Takasaki,¹⁰ K. Tamai,¹⁰ N. Tamura,³² K. Tanabe,⁴⁸ M. Tanaka,¹⁰ G. N. Taylor,²³

Y. Teramoto,³³ X. C. Tian,³⁶ S. Tokuda,²⁴ S. N. Tovey,²³ K. Trabelsi,⁹ T. Tsuboyama,¹⁰
T. Tsukamoto,¹⁰ K. Uchida,⁹ S. Uehara,¹⁰ T. Uglov,¹⁴ K. Ueno,²⁹ Y. Unno,³ S. Uno,¹⁰
Y. Ushiroda,¹⁰ G. Varner,⁹ K. E. Varvell,⁴³ S. Villa,²⁰ C. C. Wang,²⁹ C. H. Wang,²⁸
J. G. Wang,⁵⁵ M.-Z. Wang,²⁹ M. Watanabe,³² Y. Watanabe,⁴⁹ L. Widhalm,¹³
Q. L. Xie,¹² B. D. Yabsley,⁵⁵ A. Yamaguchi,⁴⁷ H. Yamamoto,⁴⁷ S. Yamamoto,⁵⁰
T. Yamanaka,³⁴ Y. Yamashita,³¹ M. Yamauchi,¹⁰ Heyoung Yang,⁴¹ P. Yeh,²⁹ J. Ying,³⁶
K. Yoshida,²⁴ Y. Yuan,¹² Y. Yusa,⁴⁷ H. Yuta,¹ S. L. Zang,¹² C. C. Zhang,¹² J. Zhang,¹⁰
L. M. Zhang,⁴⁰ Z. P. Zhang,⁴⁰ V. Zhilich,² T. Ziegler,³⁷ D. Žontar,^{21,15} and D. Zürcher²⁰

(The Belle Collaboration)

¹*Aomori University, Aomori*

²*Budker Institute of Nuclear Physics, Novosibirsk*

³*Chiba University, Chiba*

⁴*Chonnam National University, Kwangju*

⁵*Chuo University, Tokyo*

⁶*University of Cincinnati, Cincinnati, Ohio 45221*

⁷*University of Frankfurt, Frankfurt*

⁸*Gyeongsang National University, Chinju*

⁹*University of Hawaii, Honolulu, Hawaii 96822*

¹⁰*High Energy Accelerator Research Organization (KEK), Tsukuba*

¹¹*Hiroshima Institute of Technology, Hiroshima*

¹²*Institute of High Energy Physics,*

Chinese Academy of Sciences, Beijing

¹³*Institute of High Energy Physics, Vienna*

¹⁴*Institute for Theoretical and Experimental Physics, Moscow*

¹⁵*J. Stefan Institute, Ljubljana*

¹⁶*Kanagawa University, Yokohama*

¹⁷*Korea University, Seoul*

¹⁸*Kyoto University, Kyoto*

¹⁹*Kyungpook National University, Taegu*

²⁰*Swiss Federal Institute of Technology of Lausanne, EPFL, Lausanne*

²¹*University of Ljubljana, Ljubljana*

²²*University of Maribor, Maribor*

²³*University of Melbourne, Victoria*

²⁴*Nagoya University, Nagoya*

²⁵*Nara Women's University, Nara*

²⁶*National Central University, Chung-li*

²⁷*National Kaohsiung Normal University, Kaohsiung*

²⁸*National United University, Miao Li*

²⁹*Department of Physics, National Taiwan University, Taipei*

³⁰*H. Niewodniczanski Institute of Nuclear Physics, Krakow*

³¹*Nihon Dental College, Niigata*

³²*Niigata University, Niigata*

³³*Osaka City University, Osaka*

³⁴*Osaka University, Osaka*

³⁵*Panjab University, Chandigarh*

³⁶*Peking University, Beijing*

³⁷*Princeton University, Princeton, New Jersey 08545*
³⁸*RIKEN BNL Research Center, Upton, New York 11973*
³⁹*Saga University, Saga*

⁴⁰*University of Science and Technology of China, Hefei*

⁴¹*Seoul National University, Seoul*

⁴²*Sungkyunkwan University, Suwon*

⁴³*University of Sydney, Sydney NSW*

⁴⁴*Tata Institute of Fundamental Research, Bombay*

⁴⁵*Toho University, Funabashi*

⁴⁶*Tohoku Gakuin University, Tagajo*

⁴⁷*Tohoku University, Sendai*

⁴⁸*Department of Physics, University of Tokyo, Tokyo*

⁴⁹*Tokyo Institute of Technology, Tokyo*

⁵⁰*Tokyo Metropolitan University, Tokyo*

⁵¹*Tokyo University of Agriculture and Technology, Tokyo*

⁵²*Toyama National College of Maritime Technology, Toyama*

⁵³*University of Tsukuba, Tsukuba*

⁵⁴*Utkal University, Bhubaneswer*

⁵⁵*Virginia Polytechnic Institute and State University, Blacksburg, Virginia 24061*

⁵⁶*Yonsei University, Seoul*

Abstract

We report on a measurement of the charmless semileptonic B decays, $B^0 \rightarrow \pi^- \ell^+ \nu$ and $B^0 \rightarrow \rho^- \ell^+ \nu$, based on 140 fb^{-1} data collected with the Belle detector at the KEKB e^+e^- asymmetric collider. In this analysis, accompanying B mesons are reconstructed from semileptonic $B \rightarrow D^{(*)} \ell \nu$ decays, which enables us to detect the signal with high purity and with marginal statistics. We found branching fractions of $\mathcal{B}(B^0 \rightarrow \pi^- \ell^+ \nu) = (1.76 \pm 0.28 \pm 0.20 \pm 0.03) \times 10^{-4}$ and $\mathcal{B}(B^0 \rightarrow \rho^- \ell^+ \nu) = (2.54 \pm 0.78 \pm 0.85 \pm 0.30) \times 10^{-4}$, where the errors are statistical, experimental systematic, systematic due to form-factor uncertainties. We present also the branching fractions in three q^2 intervals; $q^2 < 8$, $8 \leq q^2 < 16$, $q^2 \geq 16 \text{ GeV}^2/c^2$, for each decay mode. Based on these results, the magnitude of the Cabibbo-Kobayashi-Maskawa matrix element V_{ub} is extracted. All of the presented results are preliminary.

PACS numbers: 12.15.Hh, 12.38.Gc, 13.25.Hw

INTRODUCTION

Exclusive $B \rightarrow X_u \ell \nu$ decays proceed via $b \rightarrow u W^-$ tree diagram with a spectator quark, and can be used to determine $|V_{ub}|$, one of the smallest and least known elements of the Cabibbo-Kobayashi-Maskawa matrix [1]. The major theoretical issue is determination of the form-factors (FF) involved in the decays.

In principle lattice QCD(LQCD) provides the most reliable calculation of FFs, but so far only quenched calculations have been available. Recently preliminary results of unquenched calculations have become reported [2, 3] so that a model-independent determination of $|V_{ub}|$ becomes feasible. Since LQCD results are available only in the high q^2 region the clean extraction of the $B \rightarrow \pi \ell \nu$ branching fraction in the high q^2 region ($\geq 16 \text{ GeV}^2/c^2$) is essential.

There have been several measurements in the past by CLEO, BaBar and Belle for the $B \rightarrow \pi \ell \nu$, $\rho \ell \nu$, $\eta \ell \nu$ and $\omega \ell \nu$ modes [4, 5, 6, 7, 8]. All of these analyses utilize the method, originally developed by CLEO, where the B decays are reconstructed by inferring the undetected neutrino momentum from the missing energy and momentum (“ ν -reconstruction method”) [4]. In the B -factory era, we may quickly improve the statistical precision by simply applying the ν -reconstruction method. However, the systematic uncertainty may soon limit the experimental uncertainty because of the poor signal-to-noise ratio.

In this paper, we present measurements of $B^0 \rightarrow \pi^- \ell^+ \nu$ and $B^0 \rightarrow \rho^- \ell^+ \nu$ decays by $D^{(*)} \ell \nu$ decay tagging, where we reconstruct the whole decay chain from the $\Upsilon(4S)$; $\Upsilon(4S) \rightarrow B_{sig} B_{tag}$, $B_{sig} \rightarrow \pi^- (\rho^-) \ell^+ \nu$ and $B_{tag} \rightarrow D^{(*)+} \ell^- \bar{\nu}$ with several $D^{(*)+}$ sub decay modes. The back-to-back correlation of the two B mesons in the $\Upsilon(4S)$ rest frame allows us to constrain the kinematics of the double semileptonic decay. Belle has presented a preliminary measurement of the inclusive $B \rightarrow X_u \ell \nu$ decay using this method [9]. While this method gives a signal detection efficiency that is significantly lower than the ν -reconstruction method because of the tagging, it allows us to detect the signal with high purity, even with a relaxed cut on the lepton momentum down to $0.8 \text{ GeV}/c$. This leads to less experimental systematic uncertainty and promises to yield the best overall precision from the large data sample being accumulated by B -factories over the next few years. We present the simultaneous extraction of $B^0 \rightarrow \pi^- \ell^+ \nu$ and $B \rightarrow \rho^- \ell^+ \nu$ and their q^2 distribution. Inclusion of the charge conjugate decays is implied throughout this paper.

DATA SET AND EXPERIMENT

The analysis is based on data recorded with the Belle detector at the asymmetric e^+e^- collider KEKB operating at the center-of-mass (c.m.) energy of the $\Upsilon(4S)$ resonance [10]. The $\Upsilon(4S)$ data set used for this study corresponds to an integrated luminosity of 140 fb^{-1} and contains 152×10^6 $B\bar{B}$ events.

The Belle detector is a large-solid-angle magnetic spectrometer that consists of a three-layer silicon vertex detector (SVD), a 50-layer central drift chamber (CDC), an array of aerogel threshold Čerenkov counters (ACC), a barrel-like arrangement of time-of-flight scintillation counters (TOF), and an electromagnetic calorimeter comprised of CsI(Tl) crystals (ECL) located inside a super-conducting solenoid coil that provides a 1.5 T magnetic field. An iron flux-return located outside of the coil is instrumented to detect K_L^0 mesons and to identify muons (KLM). The detector is described in detail elsewhere [11].

A detailed Monte Carlo (MC) simulation, which fully describes the detector geometry and

response and is based on GEANT [12], is applied to estimate the signal detection efficiency and to study the background. To examine the FF dependence, MC samples for the $B^0 \rightarrow \pi^-(\rho^-)\ell^+\nu$ signal decays are generated with different form-factor models; a quark model (ISGW II [13]), light cone sum rules (LCSR; Ball'01 for $\pi^-\ell^+\nu$ [14] and Ball'98 for $\rho^-\ell^+\nu$ [15]) and a quenched lattice QCD (UKQCD [16]). A relativistic quark model (Melikhov [17]) is also used for $\rho^-\ell^+\nu$. To model the cross-feed from other $B \rightarrow X_u\ell\nu$ decays, MC samples are generated with the ISGW II model for the resonant components and the DeFazio-Neubert model [18] for non-resonant component ($\pi\ell\nu$ and $\rho\ell\nu$ components are excluded in this sample). A MC sample for the $B^0 \rightarrow D^{*-}\ell^+\nu$ decay, to be used for calibration as described later, is also prepared. To model the $B\bar{B}$ and continuum backgrounds, large generic $B\bar{B}$ (based on QQ98 [19]) and $q\bar{q}$ Monte Carlo samples are used.

EVENT RECONSTRUCTION AND SELECTION

Charged particle tracks are reconstructed from hits in the SVD and CDC. They are required to satisfy track quality cuts based on their impact parameters relative to the measured profile of the interaction point (IP profile) of the two beams. Charged kaons are identified by combining information on ionization loss (dE/dx) in the CDC, Čerenkov light yields in the ACC and time-of-flight measured by the TOF system. For the nominal requirement, the kaon identification efficiency is approximately 88% and the rate for misidentification of pions as kaons is about 8%. Hadron tracks that are not identified as kaons are treated as pions. Tracks satisfying the lepton identification criteria, as described later, are removed from consideration.

Neutral pions are reconstructed using γ pairs with an invariant mass between 117 and 150 MeV/ c^2 . Each γ is required to have a minimum energy deposit of $E_\gamma \geq 50$ MeV. K_S^0 mesons are reconstructed using pairs of charged tracks that have an invariant mass within ± 7.6 MeV/ c^2 of the known K_S^0 mass.

Electron identification is based on a combination of dE/dx in CDC, the response of ACC, shower shape in ECL and the ratio of energy deposit in ECL to the momentum measured by the tracking system. Muon identification by KLM is performed by resistive plate counters interleaved in the iron yoke. The lepton identification efficiencies are estimated to be about 90% for both electrons and muons in the momentum region above 1.2 GeV/ c . where leptons from the prompt B decays dominate. The hadron misidentification rate is measured using reconstructed $K_S^0 \rightarrow \pi^+\pi^-$ and found to be less than 0.2% for electrons and 1.5% for muons in the same momentum region.

For the reconstruction of $B_{tag} \rightarrow D^{(*)+}\ell^-\bar{\nu}$, the lepton candidate is required to have the right sign charge with respect to the D meson flavor and the laboratory momentum greater than 1.0 GeV/ c ($p_\ell^{lab} > 1.0$ GeV/ c). The $D^{(*)+}$ candidates are reconstructed by using four decay modes of $D^+ - D^+ \rightarrow K^-\pi^+\pi^+$, $K^-\pi^+\pi^+\pi^0$, $K_S^0\pi^+$ and $K_S^0\pi^+\pi^0$ - and six decay modes of $D^0 - K^-\pi^+$, $K^-\pi^+\pi^0$, $K^-\pi^+\pi^+\pi^-$, $K_S^0\pi^0$, $K_S^0\pi^+\pi^-$, $K_S^0\pi^+\pi^-\pi^0$. The candidates are required to have an invariant mass m_D within $\pm 2\sigma$ (σ is a standard deviation) of the nominal D mass, where the mass resolution σ is dependent on the decay mode. D^{*+} mesons are reconstructed by combining the D^0 candidate and a pion, $D^{*+} \rightarrow D^0\pi^+$ and $D^{*+} \rightarrow D^+\pi^0$. They are required to have the mass difference $\Delta m = m_{\bar{D}\pi} - m_{\bar{D}}$ within $\pm 2\sigma$ of the nominal values.

For the reconstruction of $B_{sig} \rightarrow X_u^-\ell^+\nu$, the lepton candidate is required to have the right sign charge with respect to the X_u system and $p_\ell^{lab} > 0.8$ GeV/ c . The X_u system

may consist of either a single charged pion or a charged pion and neutral pion candidate, and the event may contain no additional charged tracks or π^0 candidates ($N_{\pi^-} = 1$ and $N_{\pi^0} \leq 1$). We also require that the residual energy from neutral clusters is less than 0.3 GeV ($E_{neut} < 0.3 \text{ GeV}$). The two leptons on the tag and the signal sides are required to have opposite charge. Loss of the signal due to $B^0 - \bar{B}^0$ mixing is estimated by the MC simulation.

We then impose a constraint from kinematics of the double semileptonic decay in the $\Upsilon(4S)$ rest frame. In the semileptonic decay on each side, $B_{1(2)} \rightarrow Y_{1(2)}\nu_{1(2)}$ ($Y_1 = D^{(*)+}\ell^-$ and $Y_2 = X_u\ell^+$), the angle between the $B_{1(2)}$ meson and the detected $Y_{1(2)}$ system $\theta_{B_{1(2)}}$ is calculated from the relation, $p_\nu^2 = (p_B - p_Y)^2 = 0$ and the known P_B (the absolute momentum of the mother B meson). This means that the $B_{1(2)}$ direction is constrained on the surface of a cone defined with the angle $\theta_{B_{1(2)}}$ around the direction of the $Y_{1(2)}$ system, as shown graphically in Figure 1. Then the back-to-back relation of the two B meson directions implies that the real B direction is on the cross lines of the two cones when one of the B system is spatially inverted. Denoting θ_{12} the angle between the $D^{*+}\ell^-$ and the $X_u\ell^+$ systems, the B directional vector $\vec{n}_B = (x_B, y_B, z_B)$ is given by, $z_B = \cos\theta_{B_1}$, $y_B = (\cos\theta_{B_2} - \cos\theta_{B_2}\cos\theta_{12})/\sin\theta_{12}$, and

$$x_B = \pm \sqrt{1 - \frac{1}{\sin^2\theta_{12}}(\cos^2\theta_{B_1} + \cos^2\theta_{B_2} - 2\cos\theta_{B_1}\cos\theta_{B_2}\cos\theta_{12})} \quad (1)$$

with the coordinate definition in Figure 1. If the hypothesis of the double semileptonic decay is correct and all the decay products are detected except for the two neutrinos, x_B^2 must range from 0 to 1. Events passing a rather loose cut $x_B^2 > -2.0$ are used for the signal extraction in the later stage of the analysis.

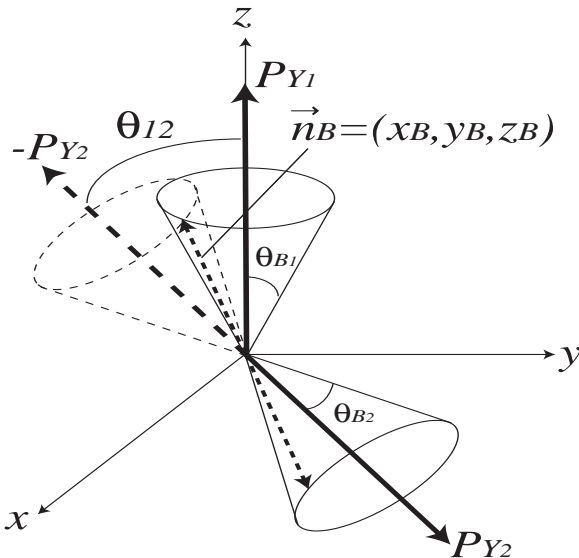


FIG. 1: Kinematics of the double semileptonic decay.

In this analysis, Eq. 1 has two solutions and the direction of the B meson is not uniquely determined. We calculate, therefore, q^2 as $q^2 = (E_{beam}^* - E_{X_u}^*)^2 - p_{X_u}^{*2}$, using the beam

energy (E_{beam}^*), energy ($E_{X_u}^*$) and momentum ($p_{X_u}^*$) of the X_u system and neglecting the momentum of the B meson in the c.m. system. The signal Monte Carlo simulation predicts that the average q^2 resolution is approximately $0.75 \text{ GeV}^2/c^2$.

According to Monte Carlo simulations, the major backgrounds come from $B^0\bar{B}^0$ events and other $B^0 \rightarrow X_u^- \ell^+ \nu$ decays, where some particles escape detection. Other backgrounds from B^+B^- events, $B^+ \rightarrow X_u^0 \ell^+ \nu$ decays and $q\bar{q}$ processes are small.

With the event selection described above, the signal MC simulation indicates that the total detection efficiency (ϵ_{total}), on the average of the electron and muon channels, is 1.5×10^{-3} for $\pi^- \ell^+ \nu$ and 8.1×10^{-4} for $\rho^- \ell^+ \nu$ with the LCSR model (Ball'01 for $\pi^- \ell^+ \nu$ and Ball'98 for $\rho^- \ell^+ \nu$). Here, ϵ_{total} is defined with respect to the number of produced $B^0\bar{B}^0$ pairs, where one B decays into the signal mode, and includes loss of the signal due to $B^0 - \bar{B}^0$ mixing. Because of the relaxed lepton momentum cut ($> 0.8 \text{ GeV}/c$), the variation of the efficiency with different FF models is relatively small; the maximum deviation from LCSR is -1.4% with ISGW II for $\pi^- \ell^+ \nu$ and $+5.5\%$ with UKQCD for $\rho^- \ell^+ \nu$.

The validity of the method to reconstruct the double semileptonic decay is checked by using the decay, $B_{sig}^0 \rightarrow D^{*-} \ell^+ \nu$ followed by $D^{*-} \rightarrow \bar{D}^0 \pi^-$, $\bar{D}^0 \rightarrow K^+ \pi^-$, with the same requirement on the tagging side. Figure 2-a) shows the obtained $M_{K\pi\pi}$ distribution and its comparison to the MC expectation. With the 140 fb^{-1} data sample, 147 ± 12 decays are clearly identified, while 165 ± 9 events are expected based on the product branching fraction $\mathcal{B}(B^0 \rightarrow D^{*-} \ell^+ \nu, D^{*-} \rightarrow \bar{D}^0 \pi^-, \bar{D}^0 \rightarrow K^+ \pi^-) = (1.40 \pm 0.07) \times 10^{-3}$ deduced from [20]. Their ratio $R = 0.89 \pm 0.08$ is used to correct the total detection efficiency ϵ_{total} for the $\pi(\rho)\ell\nu$ signals predicted by the signal MC simulations. Figure 2-b) shows the comparison of the reconstructed x_B^2 distribution using the same sample to the MC simulation. The agreement between the data and MC demonstrates the validity of the present measurement.

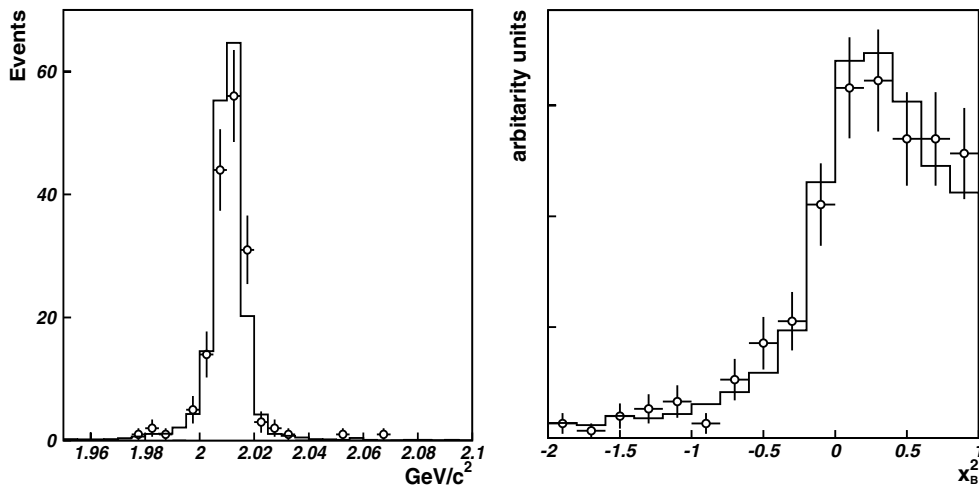


FIG. 2: Reconstructed $M(K\pi\pi)$ distribution(left) and x_B^2 distribution(right) for the $D^{*-} \ell^+ \nu$ calibration decay. Open circle is data and histogram is signal MC.

EXTRACTION OF BRANCHING FRACTIONS

The $B^0 \rightarrow \pi^- \ell^+ \nu$ and $B^0 \rightarrow \rho^- \ell^+ \nu$ signals are extracted by fitting the obtained two-dimensional distribution in (x_B^2, M_X) , where M_X is the invariant mass of the X_u system. Here, the fit components are the two signal modes; $B^0 \rightarrow \pi^- \ell^+ \nu / \rho^- \ell^+ \nu$, the other $B^0 \rightarrow X_u^- \ell^+ \nu$ background and the $B\bar{B}$ background. The PDF (probability distribution function) for each component is deduced from the MC simulation. The $\pi^- (\rho^-) \ell^+ \nu$ signal events exhibit characteristic behavior in both of their x_B^2 and M_X distributions; other $B^0 \rightarrow X_u^- \ell^+ \nu$ events exhibit a weak peaking structure in x_B^2 but a relatively flat distribution in M_X ; the $B\bar{B}$ background events are distributed uniformly in both variables. The total inclusive branching fraction $\mathcal{B}(B \rightarrow X_u \ell \nu)$ is constrained to be 0.25% [21].

Figure 3 presents the projection on M_X and x_B^2 of the fitting result for the data in the whole q^2 region. The extracted yields for the signal components are $N(\pi^- \ell^+ \nu) = 72 \pm 11$ and $N(\rho^- \ell^+ \nu) = 59 \pm 15$, with the LCSR model used for the two signal PDF.

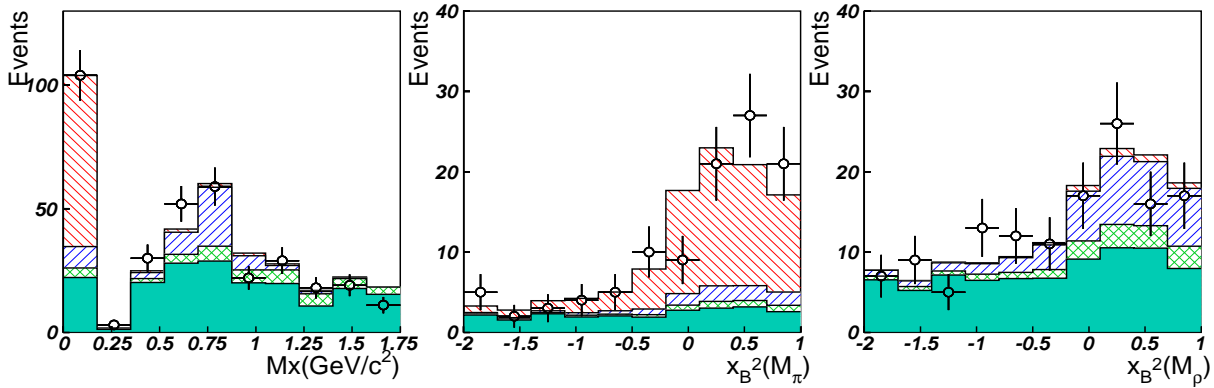


FIG. 3: Projected M_X distribution(left) and x_B^2 distributions for the mass region of π^- ($M_X < 0.18 \text{ GeV}/c^2$, middle) and ρ^- ($0.53 < M_X < 1.1 \text{ GeV}/c^2$, right) in all q^2 region; open circle is data. Histogram components are $\pi^- \ell^+ \nu$ (red 135° hatch), $\rho^- \ell^+ \nu$ (blue 45° hatch), other $X_u \ell^+ \nu$ (green cross-hatch) and $B\bar{B}$ background (bluish green shaded).

Figure 4 shows projections of the data, separated into three q^2 bins, $8 \leq q^2 < 16 \text{ GeV}^2/c^2$ and $q^2 \geq 16 \text{ GeV}^2/c^2$. Here the normalization of the other $B^0 \rightarrow X_u^- \ell^+ \nu$ and the $B\bar{B}$ background components are fixed to those obtained in the above fitting for the whole q^2 region. Table I and Table II summarize the extracted branching fractions with different FF-models for the $\pi^- \ell^+ \nu$ and $\rho^- \ell^+ \nu$, respectively. The results are unfolded using an efficiency matrix that relates the true and reconstructed q^2 for the three q^2 intervals. We calculate the total branching fraction by taking sum of the branching fractions in the three q^2 intervals.

Table III summarizes the considered experimental systematic errors for the branching fractions. The total systematic error is the quadratic sum of all individual ones. A major contribution comes from the efficiency calibration with the $B_{sig} \rightarrow D^{*-} \ell^+ \nu$ sample, where 8.3% originates from the statistics of the detected $D^{*-} \ell^+ \nu$ decays and 4.9% from the error on $\mathcal{B}(B^0 \rightarrow D^{*-} \ell^+ \nu)$ quoted in [20]. We consider the uncertainty in the number of $B^0 \bar{B}^0$ pairs; the ratio of $B^+ B^-$ to $B^0 \bar{B}^0$ pairs (f_+/f_0 , 2.4%), the mixing parameter (χ_d , 1.0%) and the measured number of $B\bar{B}$ pairs ($N_{B\bar{B}}$, 0.5%).

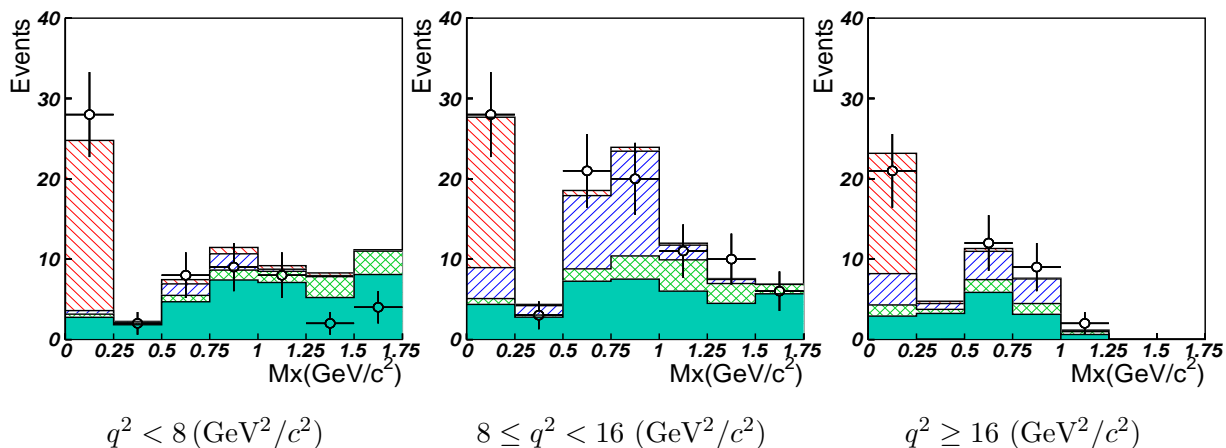


FIG. 4: Projected M_X distribution in each q^2 region; Open circle is data. Histogram components are $\pi^- \ell^+ \nu$ (red 135° hatch), $\rho^- \ell^+ \nu$ (blue 45° hatch), other $X_u \ell^+ \nu$ (green cross-hatch) and $B\bar{B}$ background (bluish green shaded).

TABLE I: Extracted branching fractions for $B^0 \rightarrow \pi^- \ell^+ \nu$ with different FF models in unit of 10^{-4} ; the total branching fraction and the partial branching fractions in three q^2 intervals. χ^2/n and the probability of χ^2 shows the quality of the fit of the FF shape to the extracted q^2 distribution.

FF model	\mathcal{B}_{total}	$\mathcal{B}_{<8}$	\mathcal{B}_{8-16}	$\mathcal{B}_{\geq 16}$	χ^2/n	Prob.
Ball'01	1.77 ± 0.28	0.72 ± 0.15	0.57 ± 0.16	0.48 ± 0.17	2.4/2	30.3%
ISGW II	1.75 ± 0.28	0.71 ± 0.15	0.60 ± 0.17	0.44 ± 0.16	1.9/2	37.8%
UKQCD	1.75 ± 0.27	0.70 ± 0.15	0.60 ± 0.16	0.45 ± 0.16	0.4/2	81.0%
Average	1.76 ± 0.28	0.71 ± 0.15	0.59 ± 0.16	0.46 ± 0.17	—	—

The systematic error due to the uncertainty on the inclusive branching fraction $\mathcal{B}(B \rightarrow X_u \ell \nu)$, which is used to constrain $X_u^- \ell^+ \nu$ background, is estimated by varying this parameter within $\pm 1\sigma$ of the error. The uncertainty on the $B\bar{B}$ background shape in our selection cut ($N_{\pi^+} = 1, N_{\pi^0} \leq 1$) is studied in the simulation by randomly removing charged tracks and π^0 according to the error in detection efficiency (1% for a charged track, 3% for π^0), and also by reassigning identified charged kaons as pions according to the uncertainty in the kaon identification efficiency (2%). The resultant change in the extracted branching fractions are assigned as a systematic error. We have seen significant change for $\rho^- \ell^+ \nu$.

The FF model dependence of the extracted branching fractions has been studied by repeating the above fitting procedure by varying the FF model for the signal mode and also for the cross-feed mode ($\pi \ell \nu \leftrightarrow \rho \ell \nu$). For the extracted $\mathcal{B}(B^0 \rightarrow \pi^- \ell^+ \nu)$, the FF model dependence is found to be small; the variation from the average is $< 0.6\%$ for the change of the $\pi \ell \nu$ FF model and $< 1.0\%$ for the change of the $\rho \ell \nu$ FF mode. As for $\mathcal{B}(B^0 \rightarrow \rho^- \ell^+ \nu)$, significant dependence on the $\rho \ell \nu$ FF model is found; the variation is $< 10.7\%$ for the change of the $\rho \ell \nu$ FF model, while it is only $< 1.3\%$ for the change of the $\pi \ell \nu$ FF model. A similar tendency was observed in the CLEO analysis [6]. At this stage, by adding linearly

TABLE II: Extracted branching fractions for $B^0 \rightarrow \rho^- \ell^+ \nu$ with different FF models in unit of 10^{-4} ; the total branching fraction and the partial branching fractions in three q^2 intervals. χ^2/n and the probability of χ^2 shows the quality of the fit of the FF shape to the extracted q^2 distribution.

FF model	\mathcal{B}_{total}	$\mathcal{B}_{<8}$	\mathcal{B}_{8-16}	$\mathcal{B}_{>16}$	χ^2/n	Prob.
Ball'98	2.59 ± 0.73	0.24 ± 0.35	1.86 ± 0.51	0.50 ± 0.39	6.3/2	4.3%
ISGW II	2.50 ± 0.86	0.18 ± 0.57	1.76 ± 0.48	0.56 ± 0.43	1.3/2	52.2%
Melikhov	2.79 ± 0.83	0.20 ± 0.29	1.88 ± 0.51	0.72 ± 0.59	8.2/2	1.6%
UKQCD	2.28 ± 0.65	0.22 ± 0.37	1.73 ± 0.46	0.33 ± 0.27	4.2/2	12.1%
Average	2.54 ± 0.78	0.21 ± 0.40	1.81 ± 0.49	0.53 ± 0.42	–	–

TABLE III: Summary of systematic errors(%) of the branching fractions

Source	$\pi^- \ell^+ \nu$	$\rho^- \ell^+ \nu$
Tracking efficiency	1	1
π^0 reconstruction	–	3
Lepton identification	2.1	2.1
Kaon identification	2	2
$D^* \ell \nu$ calibration	9.8	9.8
$Br(X_u \ell \nu)$ in the fitting	0.2	3.4
$B\bar{B}$ background shape	4.4	31.5
$N_{B\bar{B}}$	0.5	0.5
f_+/f_0	2.4	2.4
χ_d	1.0	1.0
total	11.5	33.5

the maximum variations with the signal and cross-feed FF models, we conservatively assign 1.6% (12%) as the systematic error due to the FF model dependence for the $\pi^- (\rho^-) \ell^+ \nu$ total branching fraction.

RESULTS

The total branching fractions are obtained by taking the simple average of the values obtained from the FF models shown in Tables I and II:

$$\mathcal{B}(B^0 \rightarrow \pi^- \ell^+ \nu) = (1.76 \pm 0.28 \pm 0.20 \pm 0.03) \times 10^{-4}, \quad (2)$$

$$\mathcal{B}(B^0 \rightarrow \rho^- \ell^+ \nu) = (2.54 \pm 0.78 \pm 0.85 \pm 0.30) \times 10^{-4}, \quad (3)$$

where the errors are statistical, experimental systematic, and systematic due to form-factor uncertainties. The obtained branching fractions are consistent with the existing measurements by CLEO for $B^0 \rightarrow \pi^- / \rho^- \ell^+ \nu$ [6] and BaBar for $B^0 \rightarrow \rho^- \ell^+ \nu$ [7], within the measurement uncertainties.

Figure 5 presents the obtained q^2 distributions for the two decay modes, overlaid with the best fits of FF shapes to the data. To be self-consistent, the shape of a particular FF model is fit to the q^2 distribution extracted with that FF model. The quality of the fit in terms of χ^2 and the probability of χ^2 , shown in Table I and II, may provide one way to discriminate among the models. At the present accuracy, we are unable to draw any conclusion on this point.

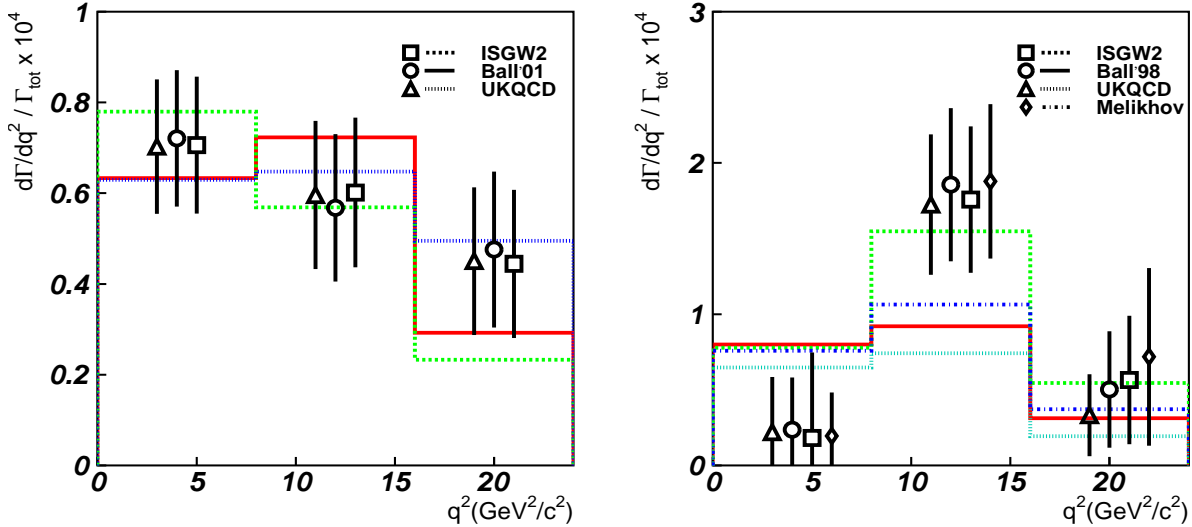


FIG. 5: Extracted q^2 distribution for the $B^0 \rightarrow \pi^- \ell^+ \nu$ (left) and $B^0 \rightarrow \rho^- \ell^+ \nu$ (right) decays. Data points are shown for different FF models used to estimate the detection efficiency. Lines are for the best fit of the FF shapes to the obtained q^2 distribution.

We extract $|V_{ub}|$ using the relation,

$$|V_{ub}| = \sqrt{\frac{\mathcal{B}(B^0 \rightarrow \pi^- (\rho^-) \ell^+ \nu)}{\tilde{\Gamma}_{thy} \tau_{B^0}}}, \quad (4)$$

where $\tilde{\Gamma}_{thy}$ is the form-factor normalization, predicted from theories. In this paper, our major focus is on the $|V_{ub}|$ determination based on the $\pi^- \ell^+ \nu$ data and the form factor predicted by LQCD calculations. Since the current LQCD calculations are available only in the region $q^2 \geq 16 \text{ GeV}^2/c^2$, we use the branching fraction in the high q^2 bin extracted with UKQCD; $\mathcal{B}_{\geq 16} = (0.45 \pm 0.16) \times 10^{-4}$. We use $\tau_{B^0} = 1.536 \pm 0.014 \text{ ps}$ for the B^0 lifetime [20].

We apply $\tilde{\Gamma}_{thy}$ predicted by the FNAL [23], JLQCD [24], APE [6] as well as UKQCD calculations, as quoted by the CLEO analysis in 2003 [6]. For the average of these results, the combined $\tilde{\Gamma}_{thy} = 1.92^{+0.32}_{-0.12} \pm 0.47 \text{ ps}^{-1}$ calculated by CLEO work is used. Here the errors are the statistical and the systematic in LQCD calculations, the latter including the quenching error of 15%. We obtain

$$|V_{ub}|_{(q^2 \geq 16)}^{\pi \ell \nu} = (3.90 \pm 0.71 \pm 0.23^{+0.62}_{-0.48}) \times 10^{-3}, \quad (5)$$

where the errors are statistical, experimental systematic, and theoretical. Figure 6 shows $|V_{ub}|$ determined with these LQCD form factor predictions. Our result is compatible and consistent with that from CLEO in 2003.

Recently, two preliminary results from the unquenched LQCD calculations were reported, FNAL'04 [2] and HPQCD [3]. Their reported $\tilde{\Gamma}_{thy}$ for the $q^2 \geq 16 \text{ GeV}^2/c^2$ region are $\tilde{\Gamma}_{thy} = 1.96 \pm 0.51 \pm 0.39 \text{ ps}^{-1}$ (FNAL'04) and $1.31 \pm 0.13 \pm 0.30 \text{ ps}^{-1}$ (HPQCD). We also estimate $|V_{ub}|$ using these calculations:

$$|V_{ub}|_{(q^2 \geq 16)}^{\pi \ell \nu} = (3.87 \pm 0.70 \pm 0.22_{-0.51}^{+0.85}) \times 10^{-3} \quad (\text{FNAL'04}), \quad (6)$$

$$|V_{ub}|_{(q^2 \geq 16)}^{\pi \ell \nu} = (4.73 \pm 0.85 \pm 0.27_{-0.50}^{+0.74}) \times 10^{-3} \quad (\text{HPQCD}). \quad (7)$$

Finally, Figure 7 summarizes the Belle $|V_{ub}|$ results from this work and from inclusive $B \rightarrow X_u \ell \nu$ measurements. The above reported results from $B^0 \rightarrow \pi^- \ell^+ \nu$ high q^2 data are in agreement with those from the inclusive $B \rightarrow X_u \ell \nu$ decays [21, 26, 27]. In the future, by accumulating more luminosity and with improvement in unquenched LQCD calculations, the present measurement will provide a more accurate determination of $|V_{ub}|$.

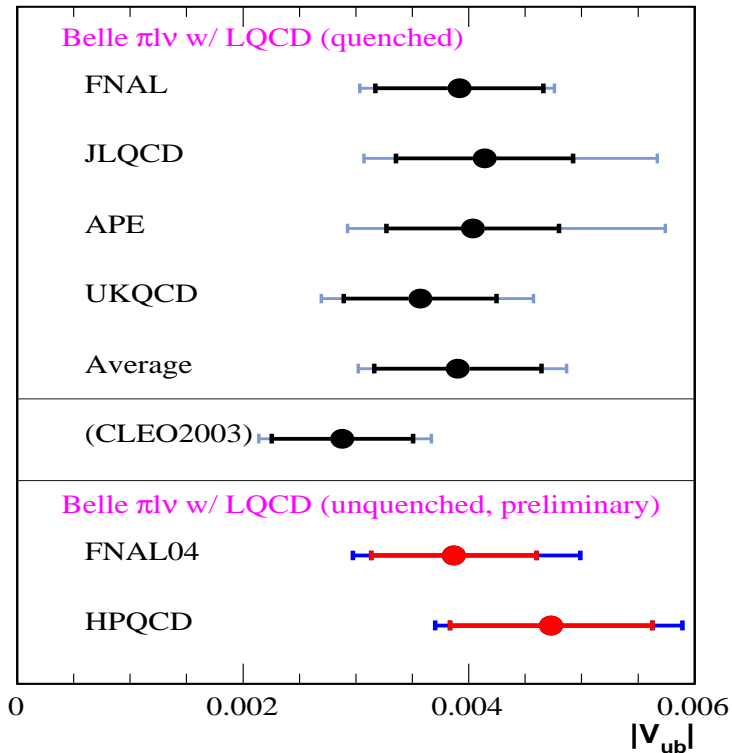


FIG. 6: $|V_{ub}|$ determined using LQCD and the $\pi^- \ell^+ \nu$ branching fraction in the $q^2 \geq 16 \text{ GeV}^2/c^2$ region. For each data point, $\pm 1\sigma$ range of the experimental errors (quadratic sum of statistical and systematic errors) and the range of the total error including the theoretical error are indicated. The CLEO result [6] with the averaged quenched LQCD formfactor is also shown for comparison.

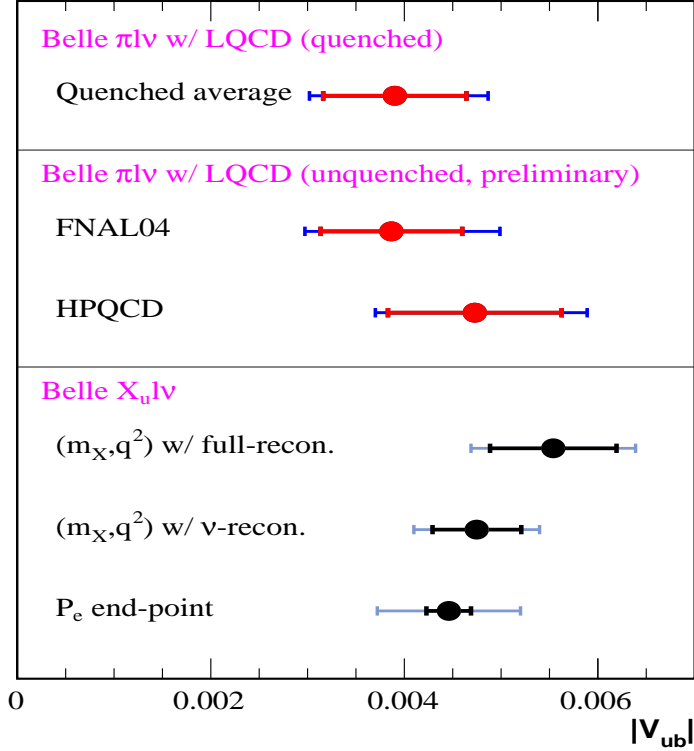


FIG. 7: Summary of Belle $|V_{ub}|$ determination. Results based on the exclusive $B^0 \rightarrow \pi^- \ell^+ \nu$ measurement ($q^2 \geq 16 \text{GeV}^2/c^2$) in this work with the averaged quenched LQCD form factor (top) and with preliminary unquenched LQCD form factors (middle two) are shown, together with those based on our inclusive $B \rightarrow X_u \ell \nu$ measurements (bottom three). The lower two inclusive results are rescaled using the recent determination of the f_u factor [28].

We thank M.Okamoto, J.Shigemitsu, S.Hashimoto and T.Onogi for useful discussions of recent lattice QCD calculations. We thank the KEKB group for the excellent operation of the accelerator, the KEK Cryogenics group for the efficient operation of the solenoid, and the KEK computer group and the National Institute of Informatics for valuable computing and Super-SINET network support. We acknowledge support from the Ministry of Education, Culture, Sports, Science, and Technology of Japan and the Japan Society for the Promotion of Science; the Australian Research Council and the Australian Department of Education, Science and Training; the National Science Foundation of China under contract No. 10175071; the Department of Science and Technology of India; the BK21 program of the Ministry of Education of Korea and the CHEP SRC program of the Korea Science and Engineering Foundation; the Polish State Committee for Scientific Research under contract No. 2P03B 01324; the Ministry of Science and Technology of the Russian Federation; the Ministry of Education, Science and Sport of the Republic of Slovenia; the National Science Council and the Ministry of Education of Taiwan; and the U.S. Department of Energy.

-
- * on leave from Nova Gorica Polytechnic, Nova Gorica
- [1] M. Kobayashi and T. Maskawa, Prog. Theor. Phys. **49**, 652 (1973).
 - [2] M. Okamoto, talk given at Lattice'04 workshop., private communication.
 - [3] J. Shigemitsu, talk given at Lattice'04 workshop., private communication.
 - [4] J. P. Alexander *et al.* (CLEO Collaboration), Phys. Rev. Lett. **77**, 5000 (1996).
 - [5] J. P. Alexander *et al.* (CLEO Collaboration), Phys. Rev. **D61**, 052001 (2000).
 - [6] S. B. Athar *et al.* (CLEO Collaboration), Phys. Rev. **D 68**, 072003 (2003).
 - [7] B. Aubert *et al.* (BaBar Collaboration), Phys. Rev. Lett. **90**, 181801 (2003).
 - [8] K. Abe *et al.* (Belle Collaboration), hep-ex/0307075.
 - [9] Talk presented by A.Sugiyama at the Moriond 2003 conference, hep-ex/0306020.
 - [10] S. Kurokawa and E. Kikutani, Nucl. Instr. and Meth. A **499**, 1 (2003), and other papers included in this volume.
 - [11] A. Abashian *et al.* (Belle Collaboration), Nucl. Instr. and Meth. A **479**, 117 (2002).
 - [12] R. Brun *et al.*, GEANT3.21, CERN Report DD/EE/84-1 (1984).
 - [13] D. Scora and N. Isgur, Phys. Rev. D **52**, 2783 (1995).
 - [14] P. Ball and R. Zwicky, JHEP **0110**, 019 (2001).
 - [15] P. Ball and V. M. Braun, Phys. Rev. D **58**, 094016 (1998).
 - [16] L. Del Debbio, J. M. Flynn, L. Lellouch, and J. Nieves (UKQCD Collaboration), Phys. Lett. B **416**, 392 (1998).
 - [17] D. Melikhov, Phys. Rev. D **53**, 2460 (1996).
 - [18] F. De Fazio and M. Neubert, JHEP **9906**, 017 (1999).
 - [19] The QQ B meson event generator was developed by the CLEO Collaboration. See the following URL: <http://www.lns.cornell.edu/public/CLEO/soft/qq>.
 - [20] Particle Data Group, Phys. Lett. B **592**, 1 (2004).
 - [21] H. Kakuno *et al.* (Belle Collaboration), Phys. Rev. Lett **92**, 071802 (2004); the inclusive branching fraction used in the fitting is based on the partial branching fraction $\Delta\mathcal{B}(B \rightarrow X_u \ell \nu; M_X < 1.7\text{GeV}/c^2, q^2 > 8 \text{ GeV}^2/c^2)$ and a recent calculation of f_u [26].
 - [22] A. Khodjamirian, R. Rückl, S. Weinzierl, C. W. Winhart, and O. I. Yakovlev, Phys. Rev. D **62**, 114002 (2000).
 - [23] A. X. Wl-Khadra, A. S. Kronfeld, P. B. Mackenzie, S. M. Ryan, and J. N. Simone, Phys. Rev. D **64**, 014502 (2001).
 - [24] S. Aoki *et al.* (JLQCD Collaboration), Phys. Rev. D **64**, 114505 (2001).
 - [25] D. Melikhov and B. Stech, Phys. Rev. D **62**, 014006 (2000).
 - [26] K. Abe *et al.* (Belle Collaboration), BELLE-CONF-0430.
 - [27] K. Abe *et al.* (Belle Collaboration), BELLE-CONF-0325.
 - [28] A.Limosani and T.Nozaki(Belle Collaboration), hep-ex/0407052.